Monthly Notices
of the
ROYAL ASTRONOMICAL SOCIETY

MNRAS **459,** 971–981 (2016)
Advance Access publication 2016 March 28

doi:10.1093/mnras/stw707

Discrepancies between CFHTLenS cosmic shear and *Planck*: new physics or systematic effects?

Thomas D. Kitching,[1⋆] Licia Verde,[2,3,4] Alan F. Heavens[5] and Raul Jimenez[2,3]

[1]*Mullard Space Science Laboratory, University College London, Holmbury St Mary, Dorking, Surrey RH5 6NT, UK*
[2]*Radcliffe Institute for Advanced Study, Harvard University, Cambridge, MA 02138, USA*
[3]*ICREA & ICC-UB, University of Barcelona, Marti i Franques 1, Barcelona E-08028, Spain*
[4]*Institute of Theoretical Astrophysics, University of Oslo, Oslo 0315, Norway*
[5]*ICIC, Astrophysics, Imperial College, Blackett Laboratory, Prince Consort Road, London SW7 2AZ, UK*

Accepted 2016 March 21. Received 2016 March 21; in original form 2016 February 9

ABSTRACT

There is currently a discrepancy in the measured value of the amplitude of matter clustering, parametrized using σ_8, inferred from galaxy weak lensing, and cosmic microwave background (CMB) data, which could be an indication of new physics, such as massive neutrinos or a modification to the gravity law, or baryon feedback. In this paper we make the assumption that the cosmological parameters are well determined by *Planck*, and use weak lensing data to investigate the implications for baryon feedback and massive neutrinos, as well as possible contributions from intrinsic alignments and biases in photometric redshifts. We apply a non-parametric approach to model the baryonic feedback on the dark matter clustering, which is flexible enough to reproduce the OWLS (OverWhelmingly Large Simulations) and Illustris simulation results. The statistic we use, 3D cosmic shear, is a method that extracts cosmological information from weak lensing data using a spherical-Bessel function power spectrum approach. We analyse the CFHTLenS weak lensing data and, assuming best-fitting cosmological parameters from the *Planck* CMB experiment, find that there is no evidence for baryonic feedback on the dark matter power spectrum, but there is evidence for a bias in the photometric redshifts in the CFHTLenS data, consistent with a completely independent analysis by Choi et al., based on spectroscopic redshifts, and that these conclusions are robust to assumptions about the intrinsic alignment systematic. We also find an upper limit, of <0.28 eV (1σ), to the sum of neutrino masses conditional on other Λ-cold-dark-matter parameters being fixed.

Key words: gravitational lensing: weak – cosmological parameters.

1 INTRODUCTION

Weak lensing of galaxy images, the effect where the observed shape of galaxies is distorted by the presence of mass perturbations along the line of sight, is a powerful probe of the matter distribution in the Universe. This is because the distortion – a change in the third eccentricity, or third flattening (known as 'ellipticity'), and size of galaxy images – depends on perturbations in the total matter density which, because we live in an apparently dark matter-dominated Universe, is in principle sensitive to the dark matter power spectrum directly. Accessing the matter power spectrum through weak lensing measurements results in a statistic that contains a wealth of cosmological information, where observations as a function of redshift can be used to infer the initial conditions of the matter perturbations, the abundance of baryonic matter (through the baryon acoustic oscillations), the linear and non-linear growth of structure, as well as the mass and hierarchy of neutrinos (e.g. Jimenez et al. 2010). In this paper we present 3D power spectrum measurements of the weak lensing effect, a statistic known as 3D cosmic shear, and use this to explore differences between the inferred matter power spectrum and that predicted by the standard ΛCDM (Λ cold dark matter) model as set by the latest cosmic microwave background (CMB) data. 3D cosmic shear is complementary to galaxy clustering measurements of the matter power spectrum that can be affected by the potentially biased mapping between the galaxy distribution and the underlying dark matter distribution.

There are several ways in which the weak lensing signal can be used to infer cosmological parameters. The most popular method to be applied to data is a real (configuration) space measurement of the 2-point statistics of the data, a correlation function, of the galaxy ellipticities either on an assumed 2D plane or in a series of

⋆ E-mail: t.kitching@ucl.ac.uk

2D redshift slices (where interslice and intraslice correlations are performed) that is referred to as 'tomography' (Hu 1999). This approach has a complicated scale and redshift-dependent sensitivity to the matter power spectrum (see e.g. Kitching, Heavens & Miller 2011; MacCrann et al. 2015). Like all correlation-function-based approaches, it does not offer a clear separation of linear versus non-linear scales which is more natural in Fourier-space. Depending on the choice of weight functions used, the observations need to be tested against predictions that necessitate accurate modelling to very small scales down to ∼300 kpc or less. On these scales poorly known effects are dominant, making accurate cosmological parameter inference extremely challenging. Such configuration-space-based measurements on recent data from the CFHTLenS (Erben et al. 2013; Heymans et al. 2013) survey have been shown to be statistically inconsistent/discrepant (colloquially referred to as being 'in tension') with recent measurements of the matter clustering from the CMB (Planck Collaboration XVI 2014). Within a standard, power-law ΛCDM model, the value of the variance of the linear matter perturbations on $8\,h^{-1}$ Mpc scales, σ_8, inferred from the weak lensing correlation-function measurements is lower than that inferred from the CMB.

There have been several studies (Battye, Moss & Pearson 2015; Dossett et al. 2015; MacCrann et al. 2015; Joudaki et al. 2016) attempting to determine the cause of this discrepancy by adding additional parameters to the likelihood analyses which describe both systematic effects in the data or in the analysis and new physics. In this paper we use an alternative 3D power spectrum approach: 3D cosmic shear.

The 3D cosmic shear method uses the 3D spherical-Bessel representation of the weak lensing galaxy ellipticities as data. The covariance of this data – the 3D power spectrum – is the quantity that contains the cosmological information. This statistic was introduced by Heavens (2003) and developed by Castro, Heavens & Kitching (2005), Heavens, Kitching & Taylor (2006), Kitching (2007), Kitching, Taylor & Heavens (2008), and Kitching et al. (2011). It was a applied to a small data set in Kitching et al. (2007), and then on a wide-field data set in Kitching et al. (2014) where several improvements to the method were also presented; including the splitting of the signal into E- and B-mode components, the application of a pseudo-C_ℓ analysis accounting for the mask in the data, and the extension of the method to include the correct correlations between the real and imaginary parts of the theoretical covariance. An investigation of the scale-dependency of the statistic was also presented, where it was shown that, by making simple scale-cuts in the data vector and theory, a self-consistent set of scales can be defined to which the signal is sensitive over all redshifts. This property makes the 3D cosmic shear approach robust to effects which are strongly scale-dependent or localized in certain k scales, such as strong non-linearities. In Kitching et al. (2014) the data set used was again CFHTLenS and it was found that when only using large scales in the statistic, more than ∼1 Mpc, results were consistent with the CMB *Planck* data – albeit with larger error-bars – but when including smaller scales of ∼0.2–1 Mpc results were no longer consistent. On small scales it was found that the amplitude of matter clustering parametrized by σ_8 was lower than that measured from *Planck* at a significance of more than 2σ.

Finding an explanation for this discrepancy with the *Planck* data is necessary, since if it were real it could be an important signature of new physics. In this paper we explore the reason for this discrepancy by extending the analysis and the modelling presented in Kitching et al. (2014). In particular we make several improvements to the statistic (as a result of computational software and hardware improvements) that allow for 10 times more angular modes, and twice as many radial modes to be included in the analysis; this results in a higher total signal-to-noise, and therefore better cosmological constraints, and an increased resolution in the angular and radial directions. We also extend the calculation to include intrinsic galaxy alignment effects (see e.g. Joachimi et al. 2015, for a review), and we test the method more extensively on simulated data that includes simulated masks, to show that the pseudo-C_ℓ approach does not introduce biases in the cosmological parameters. We extend the cosmological model that is fitted to the data to include the possibility of massive neutrinos, and also include a parametrization for small-scale departures from the dark matter-only power spectrum caused by the presence of baryons. Finally we include systematic nuisance parameters to encode potential photometric redshift biases.

In this paper we will pay particular attention to the scale dependence of changes in the matter power spectrum on small-scales $k \simeq 1.5$–$5h$ Mpc^{-1} (physical scales of ∼1 Mpc). The power spectrum can be delimited into various regions as a function of scale that reflects the dominant physics at play which must be included to model its functional form: on the very largest scales $k < 0.1\,h$ Mpc^{-1} the amplitude of matter clustering is dominated by linear physics evolving the initial primordial density fluctuations in the early universe; on intermediate scales $k \sim 0.5$–$1\,h$ Mpc^{-1} gravitational collapse of the dark matter dominates, this is a non-linear process but can be investigated using analytical techniques and N-body simulations; then on the smallest scales of 1 Mpc and less in the highly non-linear regime ($k > 1\,h$ Mpc^{-1}) non-gravitational effects driven by the baryonic content of the Universe may begin to dominate. This effect is expected to develop as galaxy evolution progresses, with the peak of the star formation rate occurring at redshifts of approximately $z \simeq 2$. Hence, the small-scale power spectrum is very poorly understood at the current time for three reasons. The first is that dark matter clustering is not well modelled: current simulations are only precise to a few per cent up to scales of ∼1 Mpc, but not below (e.g. Lawrence et al. 2010). The second is that the ΛCDM paradigm could break down at small scales and new physical processes could be present, for example some modified gravity models, neutrino physics, and warm dark matter models have signatures at scales smaller than 1 Mpc. The third is that baryonic feedback processes may dominate on scales smaller than 1 Mpc (e.g. van Daalen et al. 2011). Of these problems the baryonic feedback process is the least well understood. On scales of 1 Mpc and less, stars, galaxies, and other baryonic components of the Universe can affect the dark matter clustering, in an unknown way. White (2004) provided a simple model to elucidate the effects of baryonic cooling on predictions of the power spectrum for weak gravitational lensing, and predicted that percent level effects may be seen. Zhan & Knox (2004) provided a mixed dark matter–baryon model that included effects of baryonic cooling and the intercluster medium; they also found that the weak lensing power spectrum would be impacted by a few per cent. Jing et al. (2006) ran a set of N-body and hydrodynamical simulations to attempt to model the impact of baryons and found that up to a 10 per cent effect could be caused on the weak lensing power spectrum. Zentner, Rudd & Hu (2008), building on the N-body simulations from Rudd, Zentner & Kravtsov (2008) proposed that the problem of baryonic feedback could be mitigated by self-calibrating weak lensing surveys i.e. adding additional (nuisance) parameters to model the impact of baryons. They used a simple toy model where only the concentration of dark matter haloes was changed, and found that cosmological parameters could be biased by up to 40 per cent using even this simple model. Mead et al. (2015) also use a physically motivated model based on the modification to halo

profiles. A significant advance was made when Schaye et al. (2010) and van Daalen et al. (2011) used the *N*-body and hydrodynamical simulations called OWLS (OverWhelmingly Large Simulations) that also included active galactic nuclei (AGN) feedback. They found that the addition of AGN could have up to a 20 per cent effect on the matter power spectrum at $k \gtrsim 5\ h\,\mathrm{Mpc}^{-1}$, other mechanisms have smaller effects, around a few per cent. Therefore there are at least three effects: baryonic cooling, the effects of the intracluster medium, and AGN. However this is by no means an exhaustive list, for example hypernovae may also impact the dark matter clustering, and each of these is not an isolated effect: feedback between these effects may also be important. In this paper we present a flexible non-parametric approach for extracting small-scale power spectrum variation from *N*-body simulations and apply this to the Illustris (Nelson et al. 2015) and OWLS simulations. We then use the functions and parameters determined by this method, as additional degrees of freedom in the likelihood analysis of the data using 3D cosmic shear.

This paper is structured as follows. In Section 2 we present the method and approach, in Section 3 we present results and discussion, and in Section 4 we present conclusions.

2 METHODOLOGY

We refer to Kitching et al. (2014) for an exposition of the analysis in this paper, and also to Kitching, Heavens & Das (2015) for the inclusion of intrinsic galaxy alignment effects. We only restate the main points of this formalism here, and refer the reader to these papers for a full and more detailed presentation of the method.

2.1 Formalism

We use a 3D spherical-Bessel representation of the galaxy ellipticity field where the transform coefficients computed on the data are

$$e_{\boldsymbol{\ell}}(k) = \sum_{\mathrm{g}} e_{\mathrm{g}}(\boldsymbol{\theta}, r) j_\ell(kr) \mathrm{e}^{-\mathrm{i}\boldsymbol{\ell}.\boldsymbol{\theta}}, \tag{1}$$

where k is a radial wavenumber, $\boldsymbol{\ell}$ is an angular wavenumber, $\boldsymbol{\theta}$ and r are vector angular and radial coordinates, respectively, with r being a comoving distance, the $j_\ell(kr)$ are spherical-Bessel functions, with $\ell = |\boldsymbol{\ell}| \gg 1$. Flat sky is assumed. This is a sum over all galaxy ellipticities $e_{\mathrm{g}}(\boldsymbol{\theta}, r)$ in a data set, labelled g, that are complex (spin-2) quantities $e_{\mathrm{g}} = e_{1,\mathrm{g}} + \mathrm{i}e_{2,\mathrm{g}}$. The resulting four transform coefficients are complex quantities, that can be weighted by ℓ-mode combinations to separate out the transform coefficients that relate to the *E*- and *B*-mode components of the ellipticity field $e^E_\ell(k)$ and $e^B_\ell(k)$, and also to remove the effects of any multiplicative systematic effect in the data measurements, as described in Kitching et al. (2014; appendix A).

The mean of these transform coefficients is zero, but the covariance is not and it is this that contains the cosmological information. The likelihood for parameters of interest ψ, assumed to be Gaussian, can be written as

$$L(\phi) = \sum_\ell \frac{1}{\pi^2 |A_\ell|^{1/2}} \exp\left[-\frac{1}{2}\sum_{ij} Z_\ell(i) A^{-1}_\ell(i,j) Z^{\mathrm{T}}_\ell(j)\right]; \tag{2}$$

the labels i and j run over a range $\{k_{\mathrm{min}}, \ldots, k_{\mathrm{max}}\}$ where k_{min} and k_{max} are the minimum and maximum k-mode values, so that for N_k elements in the k-mode range the sums are over $2N_k$ modes. $Z_\ell(i) = (e^E_\ell(k), e^{E*}_\ell(k))^{\mathrm{T}}$ is a concatenation of $e^E_\ell(k)$ and $e^{E*}_\ell(k)$, both of which are vectors N_k in length. The affix-covariance matrix accounts for the complex, and correlated, nature of the spherical-Bessel transform of the ellipticity field and is equal to

$$A_\ell(i,j) = \begin{pmatrix} \Gamma & R \\ R^{\mathrm{T}} & \Gamma^* \end{pmatrix}, \tag{3}$$

which is made of four blocks of $N_k \times N_k$ matrices that are

$$\begin{aligned} \Gamma_\ell(k,k') &= \mathbb{R}[C_\ell(k,k')] + \mathbb{I}[C_\ell(k,k')] \\ R_\ell(k,k') &= \mathbb{R}[C_\ell(k,k')] - \mathbb{I}[C_\ell(k,k')], \end{aligned} \tag{4}$$

where Γ is a covariance matrix and R is a relation matrix. The matrix $C_\ell(k,k')$ is the complex covariance of the predicted signal (predicted covariance of the *E*-mode spherical-Bessel transform coefficients), which is a combination of signal and noise terms

$$C_\ell(k,k') = \widetilde{C}_\ell(k,k') + N_\ell(k,k'), \tag{5}$$

where the noise term $N_\ell(k,k')$ is given by equation 3 in Kitching et al. (2014). The signal part is a pseudo-C_ℓ estimator of the predicted covariance that accounts for the masking of the data through a multiplication with a 3D mixing matrix $M^{\mathrm{3D}}_{\ell\ell'}$ via

$$\widetilde{C}_\ell(k,k') = \left(\frac{\pi}{2}\right)^2 \sum_{\ell'} \left(\frac{\ell'}{\ell}\right) M^{\mathrm{3D}}_{\ell\ell'} C^{\mathrm{S}}_\ell \left(k\frac{\ell'}{\ell}, k'\frac{\ell'}{\ell}\right). \tag{6}$$

The original signal covariance C^{S}_ℓ can be derived using the relationship between the lens potential and the Newtonian potential integrated along the line of sight, and linking the Newtonian potential to the underlying matter perturbations via Poisson's equation. The dependence on cosmological parameters comes through the C^{S}_ℓ. This results in a predicted complex covariance that is a combination of terms from the intrinsic galaxy ellipticity and additional cosmic shear.

The observed ellipticity is a combination of the intrinsic (unlensed) galaxy ellipticity e^{I} and the additional ellipticity caused by the weak gravitational lensing along the line of sight called shear γ. In the case that $|\gamma| \ll |e^{\mathrm{I}}|$ then the observed ellipticity is a linear sum of these quantities $e = e^{\mathrm{I}} + \gamma$, which means that when taking the covariance of the observed shear transform coefficients the result is four terms that correspond to the quadratic combination of the intrinsic ellipticity and the shear (see Kitching et al. 2015):

$$\begin{aligned} C^{\mathrm{S}}_\ell(k,k') = {} & C^{\gamma\gamma}_\ell(k,k') + C^{\mathrm{II}}_\ell(k,k') \\ & + C^{\mathrm{I}\gamma}_\ell(k,k') + C^{\gamma\mathrm{I}}_\ell(k,k'). \end{aligned} \tag{7}$$

Here the superscript refers to the terms that are included in each covariance. The last term – the correlation between a foreground galaxy's observed shear and a background galaxy's intrinsic ellipticity – is expected to be zero by construction, but we include it in all calculations as redshift uncertainty can reverse the order of the assumed distances, and cause the observed correlation to be non-zero. The power spectrum for quantities X and Y, which in this case are either I or γ, can be written as a matrix multiplication:

$$C^{XY}_\ell = \widetilde{G}^X_\ell \widetilde{G}^{\dagger,Y}_\ell \tag{8}$$

where $\dagger$ refers to a transpose and complex conjugate and the matrices $\widetilde{G}^X_\ell$ are

$$\widetilde{G}^X_\ell(k,k') = D\mathcal{A}\frac{(\Delta k)^{1/2}}{k} G^X_\ell(k,k'), \tag{9}$$

where Δk is a resolution in the radial wavenumber that approximates an integral, $D = D_1 + \mathrm{i}D_2$ is a complex variable where $D_1 = \frac{1}{2}(\ell^2_y - \ell^2_x)$ and $D_2 = -\ell_x\ell_y$, where ℓ_x and ℓ_y refer to the wavenumber components in the x and y Cartesian coordinate frame.

$\mathcal{A} = 3\Omega_{\rm M}H_0^2/(\pi c^2)$ where H_0 is the current value of the Hubble parameter, $\Omega_{\rm M}$ is the ratio of the total matter density to the critical density, and c is the speed of light in a vacuum. The G matrices are different for the intrinsic and shear parts of the covariance.

For shear the G matrix is

$$G_\ell^\gamma(k,k') = \int {\rm d}z_{\rm p}{\rm d}z'\, j_\ell(kr[z_{\rm p}])n(z_{\rm p})p(z'|z_{\rm p})U_\ell^\gamma(r[z'],k'), \quad (10)$$

where $n(z_{\rm p}){\rm d}z_{\rm p}$ is the number of galaxies in a spherical shell of radius $z_{\rm p}$ and thickness ${\rm d}z_{\rm p}$, $p(z'|z_{\rm p})$ is the probability of a galaxy at redshift z' to have a photometric redshift $z_{\rm p}$, $j_\ell(kr)$ are spherical-Bessel functions.

The matrix U is

$$U_\ell^\gamma(r[z],k) = \int_0^{r[z]} {\rm d}r' \frac{F_K(r,r')}{a(r')} j_\ell(kr')P^{1/2}(k;r'), \quad (11)$$

where $P(k;r)$ is the matter power spectrum at comoving distance r at radial wavenumber k; we refer the reader to Castro et al. (2005) for a discussion of the approximation involved in using the square root of the power spectrum here. $F_K = S_K(r-r')/S_K(r)/S_K(r')$ is the lensing kernel where $S_K(r) = \sinh(r), r, \sin(r)$ for cosmologies with spatial curvature $K = -1, 0, 1$, and $a(r)$ is the dimensionless scale-factor at the cosmic time related to the look-back time at comoving distance r. The combination of the G and U matrices create the covariance of the $\gamma_E(k,\ell)$ spherical-Bessel transform coefficients where $C_\ell^{\gamma\gamma}(k,k') = \langle\mathbb{R}[\gamma_E(k,\ell)]\mathbb{R}[\gamma_E(k',\ell)]\rangle$; the same expression is true for imaginary parts $\mathbb{I}[\gamma_E(k,\ell)]$ and in the likelihood both terms are contributors. Throughout this investigation we use CAMB[1] to calculate the matter power spectra with the HALOFIT (Smith et al. 2003) non-linear correction and the module for Parametrized Post-Friedmann (PPF) prescription for the dark energy perturbations (Hu & Sawicki 2007; Fang, Hu & Lewis 2008a; Fang et al. 2008b)[2].

For the unlensed part of the galaxy ellipticity, we use the linear alignment model of Hirata & Seljak (2004), where the intrinsic galaxy ellipticity is linearly related to the local second derivative of the primordial Newtonian potential. This propagates through to a spherical-Bessel covariance, as described in Kitching et al. (2015). In this case the G matrix is

$$G_\ell^{\rm I}(k,k') = \int {\rm d}z_{\rm p}{\rm d}z'\, j_\ell(kr[z_{\rm p}])n(z_{\rm p})p(z'|z_{\rm p})\frac{U_\ell^{\rm I}(r[z'],k')}{r^2[z']}, \quad (12)$$

where

$$U_\ell^{\rm I}(r[z],k) = \int_0^{r[z]} {\rm d}r' \frac{\delta^D(r'-r)I(r'[z])}{a(r')} j_\ell(kr')P^{1/2}(k;r'), \quad (13)$$

and the factor $I(z[r])$ is

$$I[r(z)] = \left(\frac{c^2}{2H_0^2}\right)\left(\frac{2.1\times10^{-3}A_{\rm IA}}{\bar{D}(z)}\right). \quad (14)$$

$A_{\rm IA}$ parametrizes the amplitude of the intrinsic alignment signal, which has been used in several forecasting papers (e.g. Kirk et al. 2015), and also fit to data using correlation-function 2-point statistics (e.g. Heymans et al. 2013). The U matrices for both the shear and intrinsic signal effectively encapsulate the redshift kernel of the signal, where the lensing geometric kernel can be seen in the shear case – the effect being a distance-weighted integral along the line of sight, and a localized delta-function in the intrinsic alignment case. $\bar{D}(z)$ is the linear growth factor.

[1] http://camb.info version 2012.

[2] This is to be consistent with the Kitching et al. (2014) analysis, although we do not actually vary the dark energy equation of state in this paper.

2.2 Implementation

The above formalism is coded in a software 3DFAST[3], which was used in Kitching et al. (2014). In this paper we present an improved analysis, as a result of software and hardware improvements used for the cosmological parameter inference. The main result of this is an increase in the number of ℓ and k modes available for the analysis. In Kitching et al. (2014) 164 independent angular modes were used. In this paper this is increased by a factor of 10–1640 independent ℓ modes over the range $\ell_{\rm min} = 360$–4970. In the radial direction we use 50 k-modes linearly sampled between 0.001 and 5 h Mpc^{-1}, for each ℓ mode. We choose $k_{\rm max} = 5\,h$ Mpc^{-1} to avoid the extremely non-linear regime of less than a few hundred kiloparsecs in comoving separation (see Section 1). This leads to 82 000 modes measured from the data, and 4.1×10^6 modes to be modelled in the covariance[4]. This choice of angular modes avoids large scales, of more than 1 deg. For the spherical-Bessel shear transform our ℓ-mode selection corresponds an angular range of 4–60 arcmin; and this mapping from ℓ-mode to real-space angle is unaffected by the choice of k modes due to the orthogonality properties of the spherical-Bessel transform. On scales larger than this Asgari et al. (2016) use a correlation-function approach (COSEBIs), and map a k-mode and redshift-dependent angular range on to ℓ, finding that $\ell = 360$–5000 in that analysis corresponds to 40–100 arcmin, and in doing so find a signature of B modes in the CFHTLenS data over those configuration-space angular scales. We avoid such scales in this analysis, and note that a full comparison between COSEBIs and spherical-Bessel weighting requires further investigation.

To test the implementation we use the CFHT N-body CLONE simulations (Harnois-Déraps, Vafaei & Van Waerbeke 2012). These simulations were made assuming a flat ΛCDM cosmology with parameters $\Omega_{\rm M} = 0.279$, $\Omega_{\rm B} = 0.046$, $n_{\rm s} = 0.96$, $h = 0.701$, and $\sigma_8 = 0.817$. Whilst not being fully 3D simulations, they are finely binned in redshift with 26 bins over the range $z = 0$–3. In each redshift bin the matter density is projected on to a 2D plane. There are 184 independent lines of sight, wherein each one weak lensing shear information is generated via ray tracing through the simulations. Importantly these simulations have realistic masking, and are tailored to mimic the survey number density, geometry, and noise properties of the CFHTLenS survey, which is the data set we use in this paper. The presence of the realistic masks means that the pseudo-C_ℓ mask-correction can be tested. In addition we supplement the CLONE simulations with realistic photometric redshift posterior probabilities: we take the photometric redshifts posterior probabilities from CFHTLenS, and then assign a posterior to each CLONE galaxy with the appropriate mean redshift; the best estimated photometric redshift is then resampled from the assigned posterior. In Fig. 1 we show the result of applying the current implementation to the simulations where we split the available lines of sight, each of 12.84 deg^2, into groups of 12 that are approximately the same total area as the CFHTLenS survey, which is 154 deg^2 (this leaves a remainder of four simulations, lines-of-sight 180–184, which we do not use), to create simulated data of the same size as used in this paper. We show the 2-parameter likelihood contours in the $(\sigma_8, \Omega_{\rm M})$ plane, marginalized over $\Omega_{\rm B}$, h, and $n_{\rm s}$ in a flat ΛCDM cosmology (see Section 2.4). We find that the likelihood analysis recovers the input cosmology in all cases.

[3] The code is available here: https://github.com/tdk111/3dfast.

[4] The current implementation of 3DFAST can compute one covariance matrix for this data set in ∼10 s on node 36 of this machine: http://hipatia.ecm.ub.es/ganglia/.

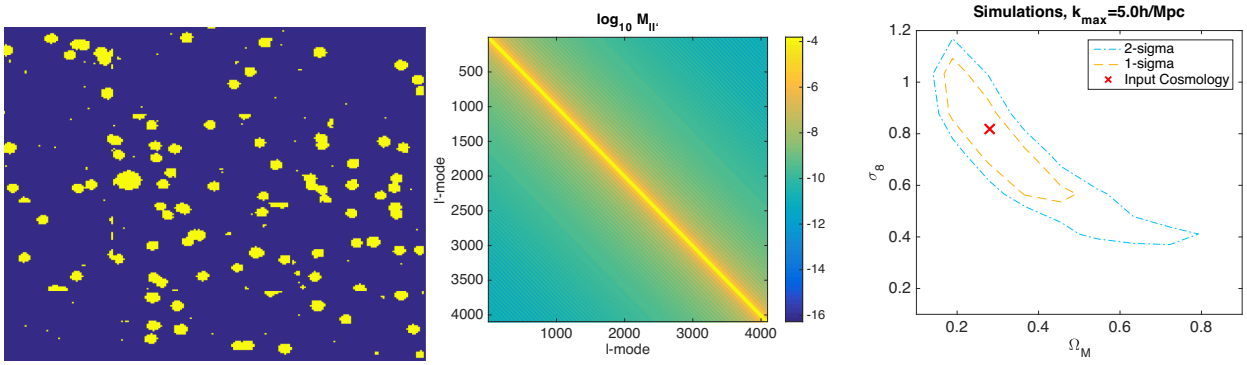

Figure 1. Left-hand panel: a typical mask in the CLONE simulations (from the line-of-sight 1, showing 12.84 deg^2), where yellow are the masked regions that simulate stellar masks. Middle panel: a typical derived mixing matrix from the simulations, where we use a maximum ℓ-mode of 4000. Right-hand panel: the mean 1σ (dashed) and 2σ (dot–dashed) contours averaged over all the simulations in the (σ_8, Ω_M) plane, compared to the input cosmology (the red cross).

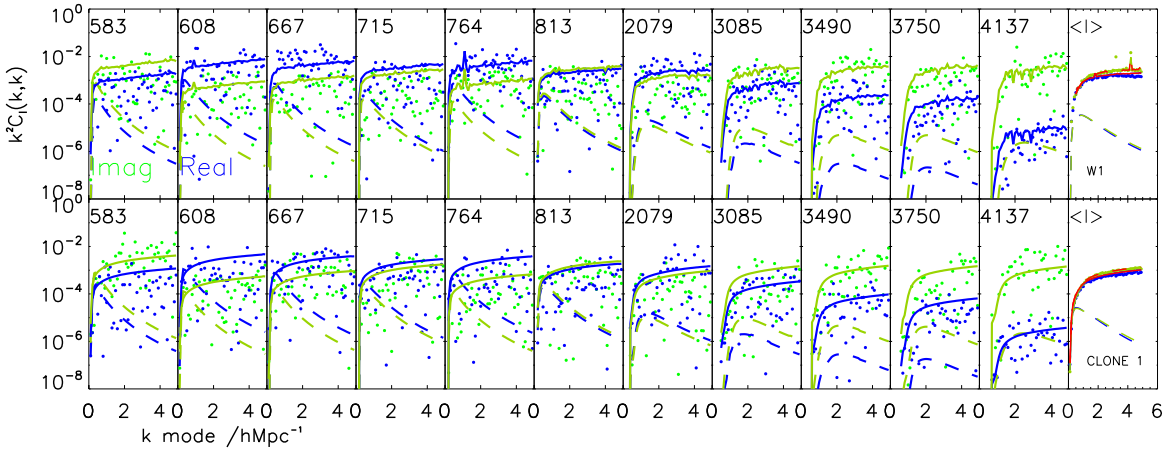

Figure 2. The real and imaginary parts of the transform coefficient data vector (blue and green points, respectively) as a function of k mode for a selection of the 1640 ℓ-modes used in the analysis, compared to the diagonal part of the expected pseudo-C_ℓ covariance matrix which is a sum of the noise part (solid lines) and the signal part (dashed lines). The rightmost panels show the mean over all ℓ modes used in the analysis. The top panels show this for the CFHTLenS $W1$ field, the bottom panels show this for the CLONE simulations line-of-sight 1.

2.3 Data

The data we use are the CFHTLenS data (Erben et al. 2013; Heymans et al. 2013), which is a 154 deg^2 optical survey (over four fields $W1$, $W2$, $W3$, $W4$) in *ugriz* bands, with weak lensing shape measurement (Miller et al. 2013) and photometric redshift posterior probabilities (Hildebrandt et al. 2012). We use the publicly available catalogues, and remove those fields that have been assessed to be unsuitable for cosmic shear analysis (Heymans et al. 2013) using star–galaxy cross-correlation statistics. This is the same data set that was used in Kitching et al. (2014).

We follow Kitching et al. (2014) in selecting only photometrically identified early-type galaxies for our analysis that are expected to have small intrinsic alignment contamination. For example, Mandelbaum et al. (2011) found a null intrinsic alignment signal in the WiggleZ data whose selection function resulted in a galaxy sample that is similar to that of CFHTLenS. In addition the linear alignment model that we use is only expected to be appropriate for early-type galaxies (see e.g. Joachimi et al. 2015).

In Fig. 2 we show the real and imaginary measured transform coefficients (equation 1) for a selection of ℓ modes as a function of k mode, and also the predicted diagonal of the pseudo-C_ℓ covariance $\widetilde{C}_\ell(k, k)$ (equation 6), for the CFHTLenS $W1$ field. We also show the same plot for one of the simulations used to test the pipeline.

Because the data we use is a 1-point estimator, and the covariance that contains the cosmological information is analytic, there is no need to estimate the covariance matrix from simulations (see e.g. Taylor, Joachimi & Kitching 2013). The primary assumption in the likelihood analysis is that the likelihood function is Gaussian, i.e. that the shear transform coefficients are Gaussian distributed. As shown in Kitching et al. (2014) this is a good approximation for the CFHTLenS data. This is also expected from the central limit theorem because if each galaxy has a posterior probability for the observed ellipticity $p_g(e) * p(\gamma)$ (where $*$ is a convolution) then the probability distribution of the shear transform coefficients, via equation (1), will be $p(e_\ell[k]) = \bigotimes_g [p_g(e) * p(\gamma)] j_\ell(kr) e^{-i\ell.\theta}$, i.e. where $\bigotimes_g$ is a series convolution over all galaxies weighted by the spherical-Bessel function, which through the central limit is expected to result in a Gaussian distribution.

2.4 Model parameters

The model parameters that we fit to the data consist of three parts that capture the cosmological model, the baryonic feedback model, and the parameters for photometric redshift systematic effects. We adopt as the baseline, the set of cosmological parameters of the flat ΛCDM model: Ω_M, Ω_B, and Ω_{DE}, the dimensionless densities of

matter, baryons, and dark energy, respectively, where we always assume a flat geometry i.e. that $\Omega_{\rm DE} = 1 - \Omega_{\rm M}$; the dark energy equation of state parameter w, that we assume to be constant with redshift; the spectral index of the initial density perturbations $n_{\rm s}$; the dimensionless Hubble parameter $h = H_0/(100\,{\rm kms}^{-1}\,{\rm Mpc}^{-1})$; the variance of matter perturbations on $8h^{-1}$ Mpc scales, σ_8; and the total sum of neutrino masses, m_ν for which we assume an inverted hierarchy throughout (the results are not sensitive to the choice of hierarchy for a data set of this size). In our investigations we will use the Planck Collaboration XVI (2014) best-fitting parameters to fix any cosmological parameters that we do not explicitly vary in the analysis, and all other parameters not listed here are also fixed at these values. Beyond the cosmological parameters we consider 'systematic' parameters (variables that parametrize systematic effects). We include the intrinsic alignment parameter $A_{\rm IA}$ as a free parameter, where we use the non-linear power spectrum in the linear alignment model; this is an ad hoc modelling of small-scale intrinsic alignment behaviour (see Blazek, Seljak & Mandelbaum 2015; Joachimi et al. 2015) but is a good empirical fit to galaxy–galaxy lensing data. For other systematic parameters we focus only on those that are most likely to have an impact on small scales. These are the impact of photometric redshifts, because photometric redshifts damp power and correlated k-modes on small radial scales less than the redshift error i.e. $k \gtrsim 2\pi/[3000\sigma_z(z)]$, where $3000\sigma_z(z)$ is approximately the comoving distance error caused by photometric redshift uncertainties at a redshift of unity (see Kitching et al. 2011, where this is explored in more detail), and baryonic feedback processes that can impact scales of $k \gtrsim 1\,h$ Mpc^{-1} (see Section 1).

2.4.1 Photometric redshift systematics

As shown in Choi et al. (2015) there is evidence from galaxy–weak lensing cross-correlations that the photometric redshifts in CFHTLenS are biased with respect to their (true) spectroscopic redshifts. We find that their bias as a function of spectroscopic redshift is well-parametrized by a linear relation; we estimate this relation from their tabulated results to be $z_{\rm bias}(z_{\rm s}) = p_2(z - p_1)$, where $p_2 = -0.19 \pm 0.05$ and $p_1 = 0.45 \pm 0.05$. To model the effect of possible redshift biases we include this redshift bias function in our analysis by shifting the CFHTLenS photometric redshift posterior distributions by this factor in equation (10), $p(z'|z_{\rm p}) \rightarrow p(z' - z_{\rm bias}|z_{\rm p})$ and letting p_1 and p_2 be free parameters, which to first order is a shift in the mean of the function.

With more data, a more complex bias function could be explored, but the limited statistical power of this data set does not warrant this. As shown in Kitching et al. (2014) the CFHTLenS data set is not large enough to support parameter estimation over more than ∼4–5 well-constrained free parameters.

2.4.2 Baryonic feedback models

We start by using the results from the OWLS (Schaye et al. 2010; van Daalen et al. 2011), a suite of large, cosmological, hydrodynamical simulations, which include various baryonic processes including AGN feedback, supernovae feedback, cooling etc. Their code uses a TREEPM algorithm to efficiently calculate the gravitational forces and smoothed particle hydrodynamics to follow and evolve the gas particles. The authors provide the matter power spectrum as a function of wavenumber k and redshift z, $P(k, z)$ (linking to equation 11 here we use $P(k, z)$ as a shorthand for $P(k; r[z])$ where $r(z)$ is the comoving distance at redshift z), for the same cosmology but with nine different baryonic effects or 'recipes'; their description can be found in table 1 of van Daalen et al. (2011; note that entries 2, 5, 6 are relative to a different cosmology and so will not be considered here). The large volume of the simulations means that the lowest k mode sampled is $0.1\,h$ Mpc^{-1}, reaching the (quasi)linear regime where baryonic effects are fully negligible.

In Zentner et al. (2013) the authors quantified the impact of baryonic effects on the convergence power spectrum using principal component analysis (PCA; see e.g. Jolliffe 1986) and found that the first two eigenmodes account for over 90 per cent of the variance among the spectra. Here we aim at using the same approach but for the matter power spectrum itself as a function of k and z.

To minimize the dependence on cosmology, we choose to model the relative change induced by the baryonic effects compared to a dark matter-only (DM ONLY) recipe; therefore we work with the quantity $R = P_i(k, z)/P_{\rm DM\,ONLY}(k, z)$, where i stands for the various baryonic recipes. We also only consider the redshift range relevant for the present analysis i.e. $0.125 \leq z \leq 1.5$.

The PCA approach describes R in terms of eigenvectors and eigenvalues:

$$R = R_{\rm mean}(k, z) + \sum_{i=1,9} V_i(k, z)\mathcal{E}_i, \tag{15}$$

where $R_{\rm mean}$ is the mean correction (the PCA-inferred mean effect of all the models considered), V_i are the eigenvectors, and $\mathcal{E}_i$ are the eigenvalues. We find that the second term in the right-hand side of equation (15) is of the same order of $R_{\rm mean}$, it cannot be neglected, but cannot change $R_{\rm mean}$ by a large factor. Our philosophy then follows Eifler et al. (2015). We describe the matter power spectrum as

$$P(k, z) = P_{\rm DM\,ONLY}(k, z)\mathcal{R}_{\vec{E}}(k, z), \tag{16}$$

with

$$\mathcal{R}_{\vec{\alpha}}(k, z) = R_{\rm mean}(k, z) + \sum_{i=1,N} V_i(k, z)\alpha_i, \tag{17}$$

where $R_{\rm mean}$ and V_i are provided by the PCA procedure (equation 15 above) and E_i their coefficients (to be determined by the data analysis). The PCA provides $N = 9$ eigenvectors but, as we shall see below, the first one or two already encode all the information one is interested in in this context. We then aim at marginalizing over the coefficients of the dominant eigenmodes. In doing so we make two fundamental assumptions here: (1) that the set of nine recipes encompasses all reasonable functional shape of the corrections (but not necessarily the amplitude) and therefore that the set of eigenmodes that the PCA analysis will yield will be a full basis set for the baryonic effects (not just a full basis set for the OWLS simulations); (2) that on scales larger than the largest scales modelled by the simulations the baryonic effects are negligible and therefore the relative effect is 0. We will completely relax the first assumption below.

We find that using only one PCA coefficient keeps the residuals below 0.5 per cent for $k < 0.5\,h$ Mpc^{-1} and below 1.2 per cent for $k < 1\,h$ Mpc^{-1}; using the first two PCAs keeps the residuals below 0.1 per cent for $k < 0.5\,h$ Mpc^{-1}. Using no PCA coefficients, only the mean correction, we find residuals below 0.8 per cent for $k < 0.5\,h$ Mpc^{-1} and below 2.5 per cent for $k < 1$. Since $R_{\rm mean}$ and V_1 are of about the same magnitude this means that the differences among the models are at least as big as the effect itself. The recipe therefore would be to set the mean correction and the first PCA eigenvector, leaving its amplitude a free parameter. One

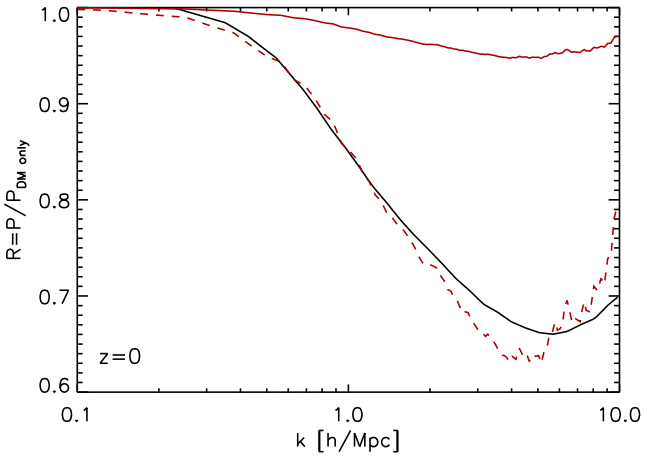

Figure 3. Comparison of OWLS and Illustris simulations' predictions for the baryonic effects on the matter power spectrum $R = P(k)/P_{\rm DM\,ONLY}(k)$ at $z = 0$. OWLS mean correction (i.e. $R_{\rm mean}$ in equation 15): upper red solid line; Illustris: lower black solid line; OWLS mean correction scaled by a factor of 7: dashed line.

would expect the recovered parameter value not to be much larger than unity for the modelling adopted to be valid.

To relax our first assumption above, we next test if this PCA description of the baryonic effects on the matter $P(k)$ shape can describe the effects found by an independent set of simulations. We use the Illustris simulation (Nelson et al. 2015) which incorporates a broad range of astrophysical processes that are believed to be relevant to galaxy formation (gas cooling, energy feedback from black holes, supernovae, AGN). While gravitational forces are calculated using a TREEPM scheme as in OWLS, the hydrodynamics are modelled by the moving-mesh technique (see Nelson et al. 2013). In particular we refer to fig. 5 of Vogelsberger et al. (2014). We find that the relative effect of baryons on the matter power spectrum, R, at $z = 0$ is seven to eight times larger than it is in the mean of the OWLS effects at the same redshift. While OWLS had nine baryonic recipes, in our PCA-based representation they are described by ∼few per cent eigenmodes around a 'mean' correction of ∼3 per cent at low redshifts at $k \sim 1\,h$ Mpc^{-1} (up to 8 per cent at higher k). Illustris on the other hand presents only one model at $z = 0$ with $|R - 1| \sim 20$ per cent at $k < 1\ h$ Mpc^{-1}(up to more than 35 per cent at larger k). No reasonable values of the OWLS-extracted PCA coefficients could reproduce such an effect; even the AGN model in van Daalen et al. (2011) gives only a ∼10 per cent suppression at $k \sim 2\ h$ Mpc^{-1}. We therefore (also) explore a model that can interpolate between the two simulations by adding a free parameter that rescales the mean correction for OWLS. This is illustrated in Fig. 3 where the power spectra ratio R at $z = 0$ are shown for the Illustris simulation, the mean correction from OWLS, $R_{\rm mean}$ in equation (15), and this correction rescaled by a factor of 7. The resulting form of the function that we fit to the data is

$$R = 1 + [R_{\rm mean}(k, z) - 1]E_1 + V_1(k, z)E_2, \qquad (18)$$

where E_1 and E_2 are free parameters, and the resulting range of the variation in the function can capture both the OWLS and Illustris behaviour.[5] Schneider & Teyssier (2015) also present an investigation of baryonic feedback behaviour, whose power spectrum suppression again requires components of order two: a suppression amplitude, and k-range at which that suppression begins to affect the power spectrum; however we have not tested our ability to recover their results.

3 RESULTS

We vary the free parameters in our analysis, and estimate their posterior probability distributions using a Metropolis–Hastings MCMC (Markov chain Monte Carlo) chain with a proposal distribution that is determined using the Fisher matrix of the parameters involved (the Fisher matrix is defined in Kitching et al. 2011). We do not assume any priors on our parameters in the analysis, except very wide boundaries to prevent the MCMC chains from moving into unphysical parameter areas, these are $\Omega_{\rm M} > 0$, $\sigma_8 > 0$, $h > 0$, $|A_{\rm IA}| < 100$.

For illustration of the tension, in Fig. 4 we show the projected 1σ and 2σ contours in the (σ_8, $\Omega_{\rm M}$) plane using maximum k-modes of $1.5\,h\,{\rm Mpc}^{-1}$ and $5\,h\,{\rm Mpc}^{-1}$ in the analysis. Note that in this figure all other cosmological parameters are fixed at the base ΛCDM *Planck* best-fitting values and the systematic parameters are at their fiducial values (no intrinsic alignment, no baryonic effects, no photo-z bias). This is compared to the *Planck* constraints[6] in the same plane. It can be seen that for (quasi-) linear scales the data is fully consistent with the *Planck* data. However there is a tension at small scales. The constraints are slightly broader than those expected from the simulated data (Fig. 1); this is because the power spectrum signal-to-noise is lower than expected due to the lower σ_8 value.

To investigate what could be causing the tension with the *Planck* constraints in the (σ_8, $\Omega_{\rm M}$) plane we fixed the ΛCDM parameters at the *Planck* maximum likelihood values, and then only varied the additional parameters in our analysis to gauge if non-canonical values of them can explain this tension, thereby placing *Planck* ΛCDM-conditional constraints on these parameters. The additional parameters are the intrinsic alignment amplitude $A_{\rm IA}$, the sum of the neutrino masses m_ν, the two baryonic feedback parameters E_1 and E_2, and the two photometric redshift bias parameters p_1 and p_2. These parameters are all varied simultaneously in the fitting, except where we explicitly fix the intrinsic alignment amplitude to be zero. By fixing all other ΛCDM parameters, including σ_8 and $\Omega_{\rm M}$, we infer the values of the additional parameters conditional on the *Planck* cosmology being correct.

In Fig. 5, and tabulated in Table 1, we show the projected constraints on each of these parameters for two cases, one where we have left the intrinsic alignment amplitude to be a free parameter in the fit, and secondly where we have fixed the intrinsic alignment amplitude to be zero. It can be seen that the data favours a very negative intrinsic alignment amplitude parameter if allowed to. This is an unphysical regime for this parameter – which should be positive if early-type galaxies are radially aligned to local dark matter overdensities, and cause a suppression in the cosmic shear power spectrum. In this analysis we also find a large photometric redshift bias, which is consistent with, but slightly more pronounced than, the results from Choi et al. (2015) which come from an entirely independent analysis of the photometric redshifts themselves. We also find that a non-zero neutrino mass (conditional on all other ΛCDM parameters being fixed) is not favoured by the data, with the analysis setting an upper limit of $m_\nu \lesssim 0.28$ eV (1σ), which is in agreement with other

[5] The PCA data and code to read in and manipulate the functions is available here: https://github.com/tdk111/baryonmodel.

[6] We use the Planck Legacy Archive chain: PLA/base/planck_lowl/base_planck_lowl_1.txt.

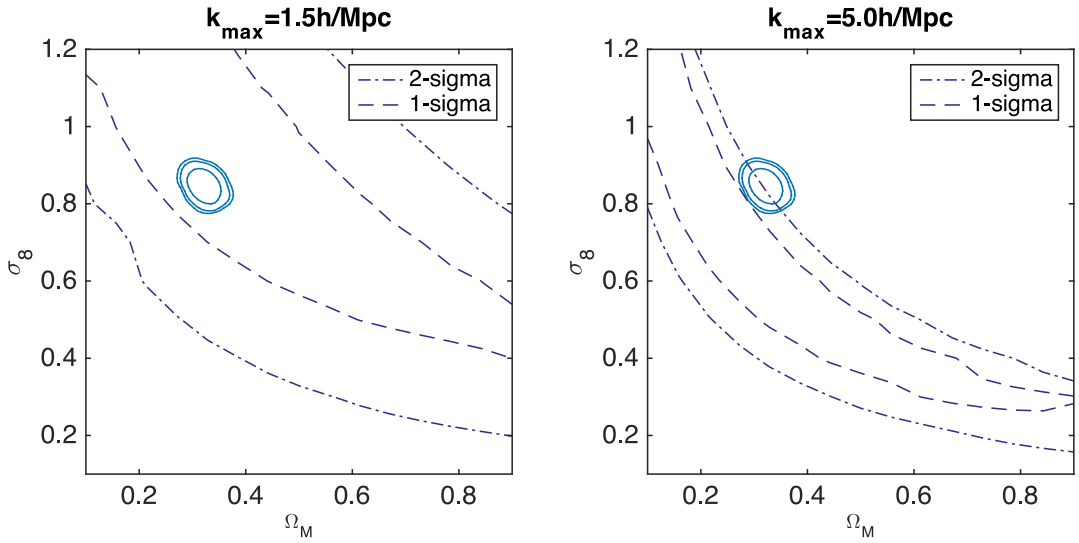

Figure 4. Projected parameter constraints for a ΛCDM cosmology in the (σ_8, Ω_M) plane showing 1σ (dashed) and 2σ (dot–dashed) contours for maximum k-modes of 1.5 h Mpc^{-1} and 5 h Mpc^{-1} in the analysis. Note that other parameters are fixed at *Planck* best-fitting values. The *Planck* 1σ, 2σ, and 3σ parameter contours are shown with the blue solid lines. Here baryonic effects, photometric redshift biases, intrinsic alignments, and neutrino mass are all assumed to be zero.

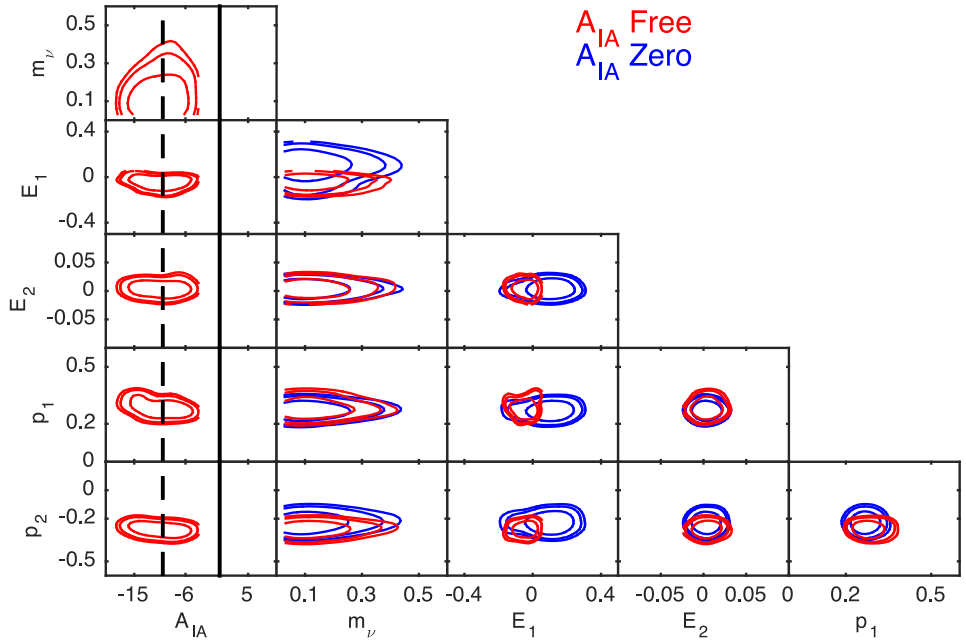

Figure 5. Projected 1σ, 2σ, and 3σ parameter constraints for the additional parameters the intrinsic alignment amplitude A_{IA}, the sum of the neutrino masses m_ν, the two baryonic feedback parameters E_1 and E_2, and the two photometric redshift bias parameters p_1 and p_2. In this analysis we use $k_{max} = 5\,h$ Mpc^{-1}. The red contours allow for a free intrinsic alignment amplitude, and the blue contours fix its value at zero. The vertical black solid and dashed lines are at $A_{IA} = 0$ and -10, respectively, for reference. Cosmological parameters are set at *Planck* best-fitting values.

recent cosmological constraints (e.g. Gonzalez-Morales et al. 2011; Verde et al. 2014; Cuesta, Niro & Verde 2015). In Figs 5 and 6 we also show the case that the intrinsic alignment amplitude is fixed to zero. This is a more physical case, as there is no strong evidence for intrinsic alignments in the early-type galaxy sample that we use in our analysis (see e.g. Mandelbaum et al. 2011; Joachimi et al. 2015). We again find that the neutrino mass is consistent with zero in this case. In Fig. 6 we show the best-fitting baryonic feedback parameters in this case, we find consistency with no baryonic feedback at all, and a tight upper limit (at 68 per cent) of 1.5 per cent, at $k = 5\,h$ Mpc^{-1}. The amplitude of the E_1 parameter indicates that the mean correction must be smaller than half of that predicted by OWLS simulations and is very far from that predicted by Illustris. This can be understood by considering equation (18). For the OWLS case E_1 should be 1 (see equation 15). For recovering the Illustris suppression E_1 should be $\sim$7 and E_2 should be small (see Fig. 3); $E_1 < 1$ implies a mean correction (i.e. a mean fractional correction to $P_{\rm DM\,only}$) smaller than in the OWLS case.

Providing a χ^2 goodness of fit estimate is not possible for our method; this is because we first vary the covariance in the

Table 1. The mean and 1σ error of the parameter constraints from CFHTLenS using the 3D cosmic shear method, assuming all other parameters are fixed at the Planck Collaboration XVI (2014) maximum likelihood values.

Intrinsic alignment	Parameter	Mean $\pm$ 1σ	
Free	$A_{\rm IA}$	-11.3 ± 5.9	
Free	m_ν/eV	0.13 ± 0.15	
Free	E_1	-0.06 ± 0.09	Baryon model
Free	E_2	0.00 ± 0.02	Baryon model
Free	p_1	0.27 ± 0.06	Photometric bias
Free	p_2	-0.29 ± 0.07	Photometric bias
Zero	m_ν/eV	0.14 ± 0.12	
Zero	E_1	0.06 ± 0.15	Baryon model
Zero	E_2	0.00 ± 0.02	Baryon model
Zero	p_1	0.26 ± 0.05	Photometric bias
Zero	p_2	-0.25 ± 0.06	Photometric bias

likelihood not the mean, and the variance will just adjust as required; therefore a Bayesian evidence calculation is required to test models correctly, but in order to implement such a test more code development of 3DFAST is required. In the meantime here we quote the likelihood values at the best-fitting *Planck* cosmology for the three cases we investigate (ΛCDM, ΛCDM-fixed-$A_{\rm IA}$ free, and ΛCDM-fixed-$A_{\rm IA}$ zero) that are indicative of level of change in information content in the fits. These are $\ln(L|\text{Planck})_{\Lambda\text{CDM}} = 17\,603$, $\ln(L|\text{Planck})_{\Lambda\text{CDM}-A_{\rm IA}-\text{free}} = 17\,607$ and $\ln(L|\text{Planck})_{\Lambda\text{CDM}-A_{\rm IA}-\text{zero}} = 17\,603$. These are as expected, higher for the $A_{\rm IA}$ case and lower for the other two cases.

The results we present are consistent with those found in Battye et al. (2015), MacCrann et al. (2015), Dossett et al. (2015), and Joudaki et al. (2016) who all investigated the CFHTLenS–*Planck* constraints. Joudaki et al. (2016) most recently found the CFHTLenS data to prefer a large and negative intrinsic alignment amplitude, a small baryonic component, and a small photometric redshift bias. A further complicating factor for correlation-function methods is the mapping of the kernel to k-space, which is more complex than for the spherical-Bessel transform. MacCrann et al. (2015) show the kernel for a fixed redshift, and Asgari, Schneider & Simon (2012) and Asgari & Schneider (2015) show that the angle-to-ℓ mode mapping can be complicated for a COSEBI weighting. A full investigation of the correlation-function k-mode sensitivity is yet to be done. However, using the Bessel function relation, appropriate for the spherical-Bessel transform used in this paper, $\ell_{\rm max} \simeq k_{\rm max} r[z]$, the range of k-modes we probe approximately corresponds to a redshift-dependent minimum angular scale of $\theta_{\rm min}[z] = 360/(k_{\rm max} r[z])$, which for $k_{\rm max} = 1.5\,h\,{\rm Mpc}^{-1}$ is $\theta_{\rm min}[z] = \{17, 4, 3\}$ arcmin for $z = \{0.2, 1.0, 1.2\}$. On the large scales the maximum angular range is also affected by the Limber function assumption, which is only applicable for $\ell_{\rm min} \gtrsim 200$ (or $\theta_{\rm max} \lesssim 100$ arcmin; Simon 2007; Loverde & Afshordi 2008), used in the theoretical interpretation of these papers' results, which we do not assume in our analysis.

The bias on photo-z obtained in Fig. 6 is similar in amount and redshift dependence to the estimated one by Niemack et al. (2009). These authors constructed different estimators of photo-z for different wavelength coverage and stellar populations models. They found that lack of inclusion of ultraviolet filters resulted in a bias on the photo-z estimated redshift. In particular, comparison of their upper panel fig. 4 with our estimated photo-z bias shows a strong resemblance over the applicable redshift ranges. The photometric bias result is robust to assumptions about the intrinsic alignments. In all cases we find that the neutrino mass constraints are unchanged, and the baryonic feedback model is consistent with zero. Furthermore as shown in Kitching et al. (2014) the ability of the CFHTLenS data to constrain any more than a handful of parameters is limited. Therefore simultaneously varying ΛCDM parameters and photometric redshift bias would result in very broad, and inconclusive, parameter constraints that we do not show in this paper.

For comparison with other surveys' cosmic shear results we note that other recent cosmic shear results are not in tension with *Planck*. In particular the Deep Lens Survey (DLS; Jee et al. 2013, Jee et al. 2015), and the Dark Energy Survey (DES; The Dark Energy Survey Collaboration et al. 2015) both find cosmic shear results (using correlation-function methodology for DLS, and correlation-function and band-power methods for DES) that are consistent with the *Planck* results. An alternative explanation for the CFHTLenS discrepancy is discussed in Liu, Ortiz-Vazquez & Hill (2016) who claim that a residual magnitude-dependent multiplicative bias can alleviate the tension.

It is interesting to note that of all the models we investigate for baryonic feedback in this paper, only OWLS AGN reproduces the gas fractions inferred from X-ray observations of clusters (see e.g. McCarthy et al. 2010). The other OWLS gas fractions are too high, while Illustris gas fractions are too low. As shown in Semboloni et al. (2011) using a halo model, the gas fractions are likely to determine the large-scale effect on the power spectrum; the smaller the gas fraction, the greater the suppression of the power spectrum on large scales (Schaye, private communication).

Therefore a suppression much smaller than that seen in the OWLS AGN output may be hard to reconcile with the X-ray observations of clusters. This means that the real tension may now be between cosmic shear and *Planck* constraints, and those from X-ray observations.

4 CONCLUSIONS

In this paper we present constraints using 3D cosmic shear, where the 3D power spectrum of weak lensing data is used to perform cosmological parameter inference. We improve this method over previous implementations by increasing the wavenumber resolution by a factor of 10. We also test this method, in particular the pseudo-C_ℓ aspect that accounted for survey masks, by applying the method to the CFHT CLONE simulations. We demonstrate that we recover the input cosmology of these simulations that have a realistic mask, and galaxy properties similar to the CFHTLenS data. We then apply this method to the CFHTLenS data, as was done in Kitching et al. (2014) and recover the result of that paper: that on linear scales $k \leq 1.5\,h\,{\rm Mpc}^{-1}$ the constraints are consistent with the *Planck* parameter constraints, but that on non-linear scales of $k \leq 5\,h\,{\rm Mpc}^{-1}$ there is a mild tension with the *Planck* data in the (σ_8, $\Omega_{\rm M}$) plane.

To investigate this tension we extend the cosmological modelling in four ways, each of which may account for an apparent drop in power at high-k, compared to ΛCDM. First we develop a model-agnostic baryonic feedback approach and apply this to the OWLS and Illustris simulations. This extracts the impact of baryonic feedback on the matter power spectrum using a PCA method; this is complementary to more analytic physically-motivated models (such as those presented in Semboloni et al. 2011; Fedeli 2014; Mead et al. 2015) but that are not guaranteed to capture all behaviour efficiently from simulations. This results in two additional parameters that describe potential matter power spectrum suppression as a function of redshift and scale. The second way we extend the method is to include intrinsic alignment modelling. For this we

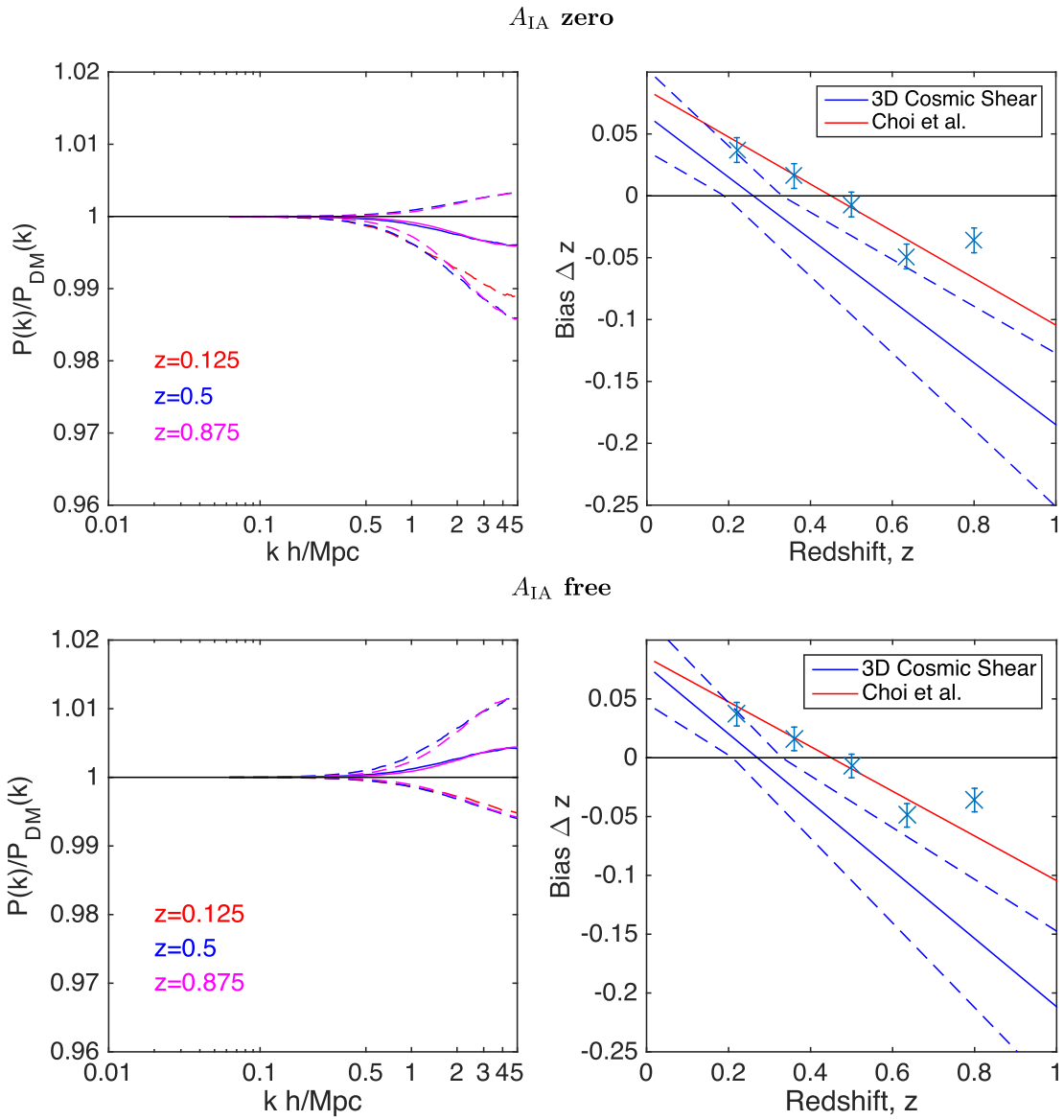

Figure 6. The best-fitting functional forms for the baryonic feedback model parameters and the photometric redshift bias parameters. For the baryonic feedback model we show the suppression for three representative redshifts. For the photometric redshift bias we also show the Choi et al. (2015) data points (crosses) and the best-fitting linear relation for these (red line). The solid blue line in the right-hand panel is the best fit from the cosmic shear constraints, and the dashed lines are the 1σ confidence regions. The legend denotes the redshifts in the left-hand panels, where the solid lines are the best functions and the dashed lines are the 1σ confidence regions. The lower panels show the results for the case that the intrinsic alignment amplitude is a free parameter (which maximises at $A_{\rm IA} \simeq -11$). The upper panels show the case in which the intrinsic alignment amplitude is set to zero.

use the linear alignment model of Hirata & Seljak (2004) with the ansatz of using the non-linear power spectrum. Thirdly we include a possible redshift-dependent photometric redshift bias. For this we use a linear form to minimize the number of free parameters, resulting in two additional parameters; however any functional form or binning in redshift could be used. Finally we include neutrino mass as an additional cosmological parameter.

We apply 3D cosmic shear to the CFHTLenS data varying the additional parameters. With the caveat that for computational reasons we keep all other parameters fixed at the *Planck* best-fitting values (although this is unlikely to be a significant issue since *Planck* errors are much smaller than those from CFHTLenS). We find that when the intrinsic alignment amplitude is allowed to vary as a free parameter the data favours a large and negative value. This is probably unphysical: the intrinsic alignment function is being used to boost the cosmic shear power, rather than suppress it as expected if tidal effects align galaxies radially near mass concentrations. In this case we also find a negligible suppression of the matter power due to baryonic feedback modelling, a large photometric redshift bias, and a small neutrino mass $\lesssim$0.28 eV. If we restrict the intrinsic alignment amplitude to be zero, which is consistent with galaxy–galaxy lensing measurements for the early-type galaxy sample we use in our analysis (see Mandelbaum et al. 2011; Joachimi et al. 2015), then we also find that the data favours a model in which there is little or no suppression of power caused by baryonic feedback effects and a large photometric redshift bias.

Conditional on the *Planck* best-fitting cosmology, and further unaccounted for systematics in the CFHTLenS data, these results rule out the baryonic feedback models in OWLS with AGN and Illustris simulations at high significance. We find this result is robust to the

amplitude of the intrinsic alignment signal and neutrino mass. To summarize: assuming *Planck* best-fitting cosmological parameters, our 3D weak lensing analysis of CFHTLenS weak lensing data shows no evidence for either non-zero neutrino masses or baryon feedback. For physically reasonable intrinsic alignments, the data indicate a significant bias in the CFHTLenS photometric redshifts, which is very similar to, and consistent with, findings of Choi et al. (2015) based on an entirely different argument from comparison with spectroscopic samples. When this bias is accounted for, the evidence for baryon feedback goes away.

In assessing cosmological large-scale-structure statistics, the critical methodological factor is the ability of methods to probe cleanly defined ranges of physical scales in the analysis. This is particularly crucial in cosmic shear analyses where several poorly understood systematic and astrophysical effects can have a large impact, and where there is potentially a wealth of cosmological information. The 3D cosmic shear approach taken in this paper can separate scales in this manner, and in addition works in the correct geometry for the data. Future optimization of this approach will improve these aspects further allowing for robust scale-dependent tests of cosmology and astrophysics and, as the volume of weak-lensing surveys increases in size (O(1000) deg^2) and depth significantly beyond the CFHTLenS data, we envision that a clear signature of neutrino physics will be unveiled in the sky (Jimenez et al. 2010).

ACKNOWLEDGEMENTS

LV thanks M. Vogelsberger for providing tabulated form of fig. 5 from Nature 509, 177 (2014). TDK is supported by a Royal Society University Research Fellowship. LV and RJ acknowledge support of Mineco grant AYA2014-58747-P, MDM-2014-0369 of ICCUB (Unidad de Excelencia 'Maria de Maeztu') and Royal Society grant IE140357. We thank the CFHTLenS, Illustris, OWLS, and *Planck* groups for making their data, catalogues, and simulations public. We thank Gabriel Perez and the system administration of the Hipatia computer. We thank Justin Alsing and Jason McEwen for useful discussions. We thank Joop Schaye, Hendrik Hildebrandt, Catherine Heymans, Peter Schneider, Aurel Schneider, Marika Asgari, Jia Liu, James Jee for comments on the text. We also thank an anonymous referee for careful review of our submission to MNRAS.

REFERENCES

Asgari M., Schneider P., 2015, A&A, 578, A50
Asgari M., Schneider P., Simon P., 2012, A&A, 542, A122
Asgari M., Heymans C., Blake C., Harnois-Deraps J., Schneider P., Van Waerbeke L., 2016, preprint (arXiv:1601.00115)
Battye R. A., Moss A., Pearson J. A., 2015, J. Cosmol. Astropart. Phys., 4, 048
Blazek J., Seljak U., Mandelbaum R., 2015, preprint (arXiv:1504.04412)
Castro P. G., Heavens A. F., Kitching T. D., 2005, Phys. Rev. D, 72, 023516
Choi A. et al., 2015, preprint (arXiv:1512.03626)
Cuesta A. J., Niro V., Verde L., 2015, preprint (arXiv:1511.05983)
Dossett J. N., Ishak M., Parkinson D., Davis T. M., 2015, Phys. Rev. D, 92, 023003
Eifler T., Krause E., Dodelson S., Zentner A. R., Hearin A. P., Gnedin N. Y., 2015, MNRAS, 454, 2451
Erben T. et al., 2013, MNRAS, 433, 2545
Fang W., Hu W., Lewis A., 2008a, Phys. Rev. D, 78, 087303
Fang W., Wang S., Hu W., Haiman Z., Hui L., May M., 2008b, Phys. Rev. D, 78, 103509
Fedeli C., 2014, J. Cosmol. Astropart. Phys., 4, 028
Gonzalez-Morales A. X., Poltis R., Sherwin B. D., Verde L., 2011, preprint (arXiv:1106.5052)
Harnois-Déraps J., Vafaei S., Van Waerbeke L., 2012, MNRAS, 426, 1262
Heavens A. F., 2003, MNRAS, 343, 1327
Heavens A. F., Kitching T. D., Taylor A. N., 2006, MNRAS, 373, 105
Heymans C. et al., 2013, MNRAS, 432, 2433
Hildebrandt H. et al., 2012, MNRAS, 421, 2355
Hirata C. M., Seljak U., 2004, Phys. Rev. D, 70, 063526
Hu W., 1999, ApJ, 522, L21
Hu W., Sawicki I., 2007, Phys. Rev. D, 76, 064004
Jee M. J., Tyson J. A., Schneider M. D., Wittman D., Schmidt S., Hilbert S., 2013, ApJ, 765, 74
Jee M. J., Tyson J. A., Hilbert S., Schneider M. D., Schmidt S., Wittman D., 2015, preprint (arXiv:1510.03962)
Jimenez R., Kitching T., Peña-Garay C., Verde L., 2010, J. Cosmol. Astropart. Phys., 5, 35
Jing Y. P., Zhang P., Lin W. P., Gao L., Springel V., 2006, ApJ, 640, L119
Joachimi B. et al., 2015, Space Sci. Rev., 193, 1
Jolliffe I. T., 1986, Principal Component Analysis. Springer-Verlag, Berlin, p. 487
Joudaki S. et al., 2016, preprint (arXiv:1601.05786)
Kirk D. et al., 2015, Space Sci. Rev., 193, 139
Kitching T. D., 2007, PhD thesis, Univ. Edinburgh
Kitching T. D., Heavens A. F., Taylor A. N., Brown M. L., Meisenheimer K., Wolf C., Gray M. E., Bacon D. J., 2007, MNRAS, 376, 771
Kitching T. D., Taylor A. N., Heavens A. F., 2008, MNRAS, 389, 173
Kitching T. D., Heavens A. F., Miller L., 2011, MNRAS, 413, 2923
Kitching T. D. et al., 2014, MNRAS, 442, 1326
Kitching T. D., Heavens A. F., Das S., 2015, MNRAS, 449, 2205
Lawrence E., Heitmann K., White M., Higdon D., Wagner C., Habib S., Williams B., 2010, ApJ, 713, 1322
Liu J., Ortiz-Vazquez A., Hill J. C., 2016, preprint (arXiv:1601.05720)
Loverde M., Afshordi N., 2008, Phys. Rev. D, 78, 123506
McCarthy I. G. et al., 2010, MNRAS, 406, 822
MacCrann N., Zuntz J., Bridle S., Jain B., Becker M. R., 2015, MNRAS, 451, 2877
Mandelbaum R. et al., 2011, MNRAS, 410, 844
Mead A. J., Peacock J. A., Heymans C., Joudaki S., Heavens A. F., 2015, MNRAS, 454, 1958
Miller L. et al., 2013, MNRAS, 429, 2858
Nelson D., Vogelsberger M., Genel S., Sijacki D., Keres D., Springel V., Hernquist L., 2013, MNRAS 429, 3353
Nelson D. et al., 2015, Astron. Comput., 13, 12
Niemack M. D., Jimenez R., Verde L., Menanteau F., Panter B., Spergel D., 2009, ApJ, 690, 89
Planck Collaboration XVI, 2014, A&A, 571, A16
Rudd D. H., Zentner A. R., Kravtsov A. V., 2008, ApJ, 672, 19
Schaye J. et al., 2010, MNRAS, 402, 1536
Schneider A., Teyssier R., 2015, J. Cosmol. Astropart. Phys., 12, 049
Semboloni E., Hoekstra H., Schaye J., van Daalen M. P., McCarthy I. G., 2011, MNRAS, 417, 2020
Simon P., 2007, A&A, 473, 711
Smith R. E. et al., 2003, MNRAS, 341, 1311
Taylor A., Joachimi B., Kitching T., 2013, MNRAS, 432, 1928
The Dark Energy Survey CollaborationAbbott T. et al., 2015, preprint (arXiv:1507.05552)
van Daalen M. P., Schaye J., Booth C. M., Dalla Vecchia C., 2011, MNRAS, 415, 3649
Verde L., Jimenez R., Simpson F., Alvarez-Gaume L., Heavens A., Matarrese S., 2014, MNRAS, 443, 122
Vogelsberger M. et al., 2014, Nature, 509, 177
White M., 2004, Astropart. Phys., 22, 211
Zentner A. R., Rudd D. H., Hu W., 2008, Phys. Rev. D, 77, 043507
Zentner A. R., Semboloni E., Dodelson S., Eifler T., Krause E., Hearin A. P., 2013, Phys. Rev. D, 87, 043509
Zhan H., Knox L., 2004, ApJ, 616, L75

This paper has been typeset from a TEX/LATEX file prepared by the author.